Structure and Evolution of Winter Cyclones in the Central United States and Their Effects on the Distribution of Precipitation. Part III: The Development of a Squall Line Associated with Weak Cold Frontogenesis Aloft

JOHN D. LOCATELLI, JONATHAN E. MARTIN, JEFFREY A. CASTLE, AND PETER V. HOBBS

Atmospheric Sciences Department, University of Washington, Seattle, Washington

(Manuscript received 24 October 1994, in final form 21 February 1995)

ABSTRACT

From 8 to 9 March 1992 cold frontogenesis aloft (CFA), which was associated with the development of a vigorous baroclinic wave, triggered a series of squall lines that produced large hail and several tornadoes as they moved across the central United States. The air lifted by the CFA, which produced the squall lines, was made potentially unstable as a result of the circulation associated with a surface drytrough. This study provides further support for the view that in winter and early spring CFA plays an important role in triggering severe weather in the central United States.

1. Introduction

Squall lines in the United States are often accompanied by severe weather and tornadoes. Surprisingly, even in the Gulf States tornadoes are most common in winter (Fujita 1992) due to the frequent occurrence of squall lines.

Early researchers struggled to understand the formation of squall lines (or "instability lines" as they were often called). Holzman (1936) and Lichtblau (1936) suggested that a majority of the events that produced significant winter precipitation in the midwest United States are associated with cold fronts aloft. Lloyd (1942) proposed that tornadic storms can develop and move northward along cold fronts aloft as the fronts move eastward. Crawford (1950) summarized the results of studies of early spring squall lines over a period of five years in Tennessee, Alabama, Georgia, and the Carolinas. He concluded "the instability line develops along the axis of a warm tongue at 850 mb after cold advection at 700 mb has reached the fore part of the associated trough and is advancing at a more rapid rate than the warm tongue." Crawford also noted "no pre-cold frontal instability lines of any importance were observed over the southeastern states without the warm tongue at 850 mb and strong cold-air advection in the fore trough at 700 mb."

Studies in the early 1950s supported the view that squall lines are linked to cold fronts aloft. Williams (1953), in a study of pressure waves (i.e., the pressure trace that a feature leaves as it moves past a station) in the central Midwest, concluded that most tornadoes are associated with what he termed "elevation type" pressure changes, which he suggested coincided with cold fronts aloft. In a study of tornadoes in Georgia, Armstrong (1953) found that most occurrences of two or more tornadoes were associated with widespread maritime tropical air covering a large area of the south and a fast-moving trough at 700 hPa with pronounced cold- and warm-air advection.

Newton (1950), in a paper dealing with the structure and mechanisms of prefrontal squall lines, stated "one of the older theories is that the squall line is a result of a cold front aloft (but) difficulty with this explanation is the frequent lack of evidence of a front aloft." Newton concluded "that the most acceptable explanation is that a mass of rain-cooled air sets up a shallow local cold front in the warm sector, which subsequently releases the thunderstorm energy ahead of the real cold front." This view received widespread acceptance, although evidence to the contrary was periodically cited. For example, Omoto (1965) studied precipitation zones ahead of surface cold fronts in winter in the central United States. He concluded that extensive precipitation zones in the "warm sector"[1] of cyclones were common and that their formation was related to synoptic-scale disturbances aloft rather than to boundary layer forcing.

Corresponding author address: Dr. Peter V. Hobbs, Department of Atmospheric Sciences, AK-40, University of Washington, Seattle, WA 98195.

[1] We have inserted quotation marks around warm sector since we believe that many of the "warm sectors" cited by Omoto are the result of the frequent misanalysis of pressure troughs as cold fronts in the south-central United States (Hobbs et al. 1990).

© 1995 American Meteorological Society

The precipitation zones were similar to "warm-sector" squall lines in that the precipitation first appeared along the western boundary of a low-level moist tongue beneath the southwesterly flow on the eastern side of a major advancing upper trough. Importantly, however, Omoto showed that the precipitation zones occurred also in association with a baroclinic, cold-air advection region at about 600 hPa.

In the 1980s an increasing body of research suggested that cold fronts, with bases above the surface, can trigger squall lines and that the motion of squall lines is connected with that of the cold air aloft. Keyser and Carlson (1984) suggested that the baroclinic zone on the western edge of the elevated mixed layer was frontogenetically active and contributed to the outbreak of severe convection along the dryline. Browning (1985) suggested that squall lines in the midwest United States might be associated with split cold-front-type structures. Locatelli et al. (1989) analyzed a cyclone that developed in the lee of the Rocky Mountains and moved eastward off the Atlantic Coast. The evolution and structure of this storm was distinctly nonclassic: it had a north–south-oriented surface occluded-like front, which evolved from the interaction of a lee trough east of the Rockies with a cold front, and rainbands parallel to and east of the occluded-like front. The rainbands were generated by a cold front aloft (Sienkiewicz et al. 1989; Geerts and Hobbs 1991). Locatelli et al. (1989) suggested that in a more convectively unstable air mass the rainbands could have developed into a squall line, which might then have been misanalyzed as a warm-sector (i.e., nonfrontal) squall line located east of a surface cold front. Martin et al. (1990) described another nonclassic cyclone structure in the central United States in which a banded region of light to moderate convective activity was coincident with a region of midlevel frontogenesis to the east of a trough.

The view that midlevel, frontogenetically active, baroclinic zones can trigger squall lines east of the Rocky Mountains is encapsulated in the *cold frontogenesis aloft* (CFA) conceptual model of Hobbs et al. (1990). In this model the term CFA refers to the leading edge of a transition zone above the surface that separates advancing cold air from warmer air. The length of the transition zone is much greater than its width, and the gradients of temperature and absolute momentum in the transition zone are much greater than in the adjacent regions. Defined in this way, the CFA encompasses features ranging from regions of concentrated upper-level cold-air advection within migrating upper shortwaves to bona fide upper-level frontal zones of the type discussed by Keyser and Shapiro (1986). The important dynamical characteristic that these features have in common is the occurrence of active frontogenesis in association with baroclinic zones (frontal or nonfrontal).

In this paper we describe the formation of a rainband that produced severe weather and numerous tornadoes as it crossed the central United States on 8–9 March 1992. We will show that this rainband was initiated along a drytrough, that is, a lee trough with characteristics of a dryline (Martin et al. 1995), under the influence of weak cold frontogenesis aloft.

In light of the results presented in this paper, and prior research on CFA, we will consider 1) the assertions of Locatelli et al. (1989) and Hobbs et al. (1990) that CFA can trigger squall lines, 2) Browning's suggestion that split cold fronts may be responsible for squall lines in the central United States, and 3) earlier studies that suggest squall lines can be triggered by CFA.

In sections 2a,b we describe the outbreaks of convection and the formation of the CFA rainband using radar, satellite, surface, and upper-air data. In section 2c we use the Pennsylvania State University–NCAR MM4 model to provide further information on the development and movement of the vertical structure of the CFA and the development of the potential instability ahead of the CFA. In section 3 we use a combination of model outputs and measurements to explore how the atmosphere became destabilized and isolated convection broke out in the southern and northern portions of the regions where the CFA rainband formed. In section 4 we propose a mechanism for the formation of the CFA rainband. The observations and ideas presented in the paper are discussed and summarized section 5.

2. Observations

a. Outbreak of convection

At 1200 UTC 8 March 1992 a vigorous short-wave trough, characterized by sharp curvature, strong baroclinicity, and diffluence at 500 hPa, was approaching the south-central United States from the southwest (Fig. 1a). As the trough moved toward the east, a surface drytrough developed (discussed in detail by Martin et al. 1995), so that, by 1800 UTC 8 March, an axis of high-equivalent-potential-temperature θ_e air (not shown) was located just to the east of the drytrough (Fig. 1b). The combination of strong upper-level forcing and potent thermodynamics is often attended by severe weather. In anticipation of this, the National Severe Storms Forecast Center (NSSFC) issued severe weather watches from north-central Texas to the Kansas–Nebraska border for the period 1900–2100 UTC 8 March (Fig. 2). These watch boxes were located immediately east of the surface position of the drytrough, and they extended along the axis of maximum θ_e at the surface.

At 2335 UTC 8 March a series of strong convective cells were present within the watch boxes, and,

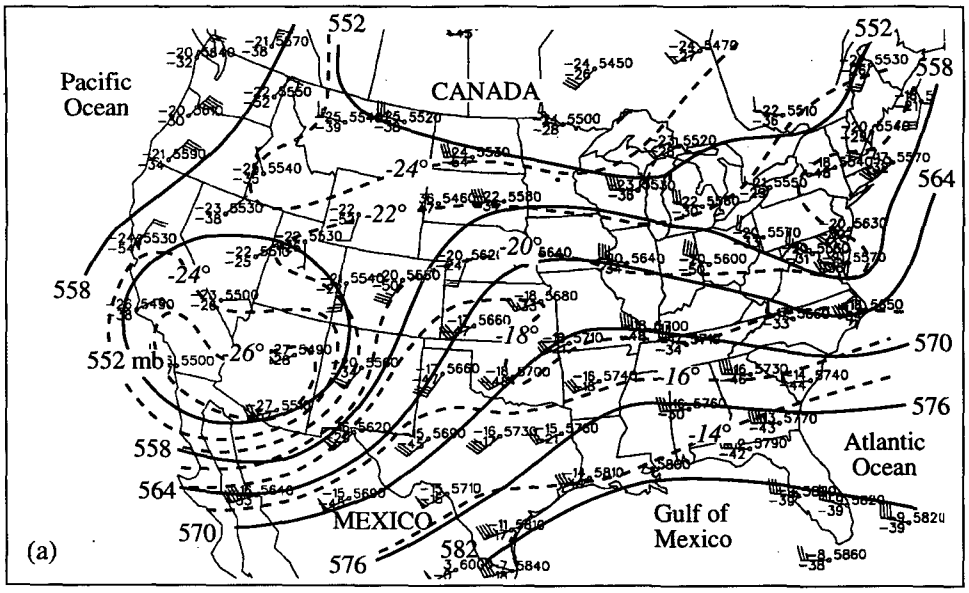

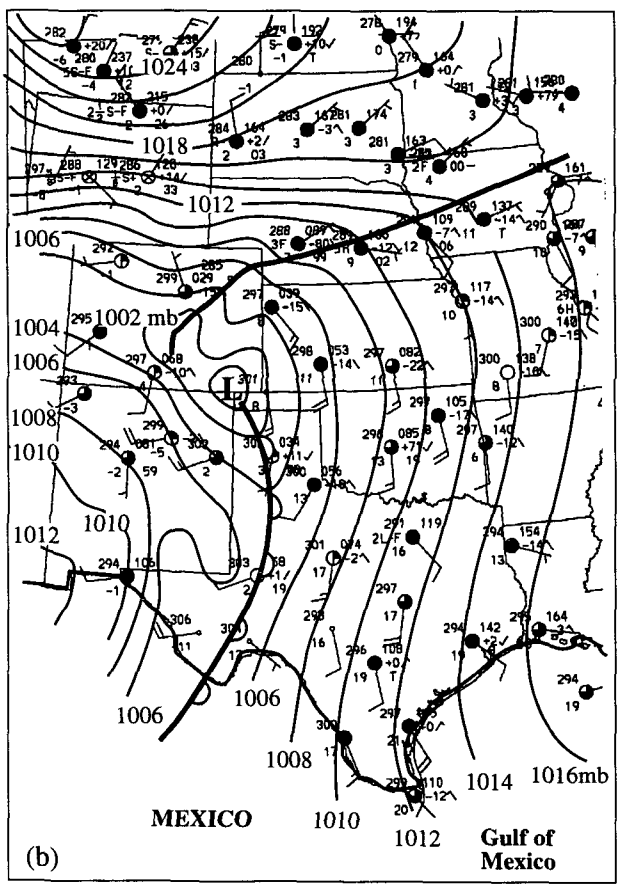

FIG. 1. (a) 500-hPa analysis at 0000 UTC 8 March 1992. Solid lines are geopotential height (dam, contoured every 6 dam). Dashed lines are isotherms (°C, contoured every 2°C). Winds speeds are indicated by short barb, 2.5 m s^{-1}; long barb, 5 m s^{-1}; flag, 25 m s^{-1}. The station data was plotted in the standard upper-level station model format. (b) Surface analysis for 1800 UTC 8 March 1992. Solid lines are isobars (hPa, contoured every 2 hPa). The heavy solid line indicates the position of the arctic front. The scalloped line indicates the position of the drytrough. Wind speeds are indicated as in (a). The surface data are plotted in the standard station model format with θ replacing temperature.

by 0235 UTC 9 March, these cells had formed a series of organized severe squall lines that stretched southward from central Kansas to the Rio Grande (Fig. 3a). By 0635 UTC 9 March the northern portions of the squall lines were located well east of the drytrough (Fig. 3b). For reasons that will become clear later, we refer to this series of squall lines as the *CFA rainband*.

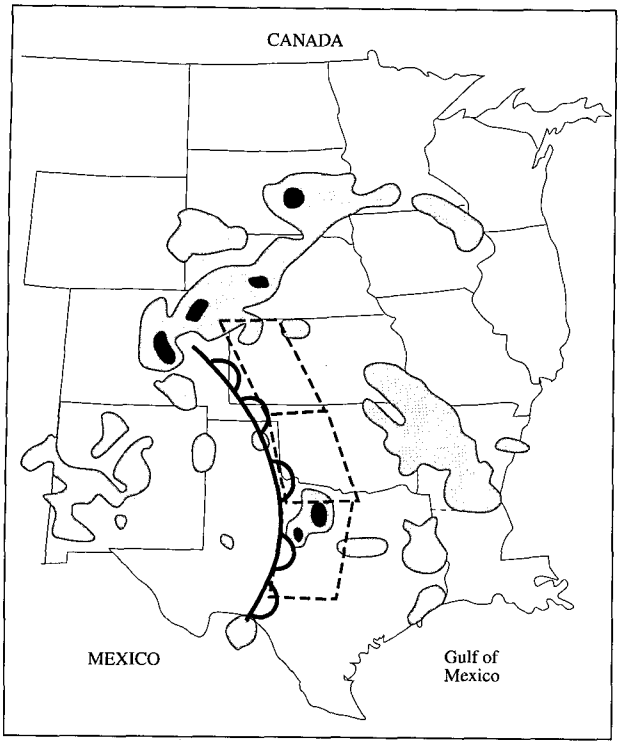

FIG. 2. National Weather Service radar summary for 2135 UTC 8 March 1992. Radar echoes are shaded with second- and third-level echoes contained within dark solid lines. The scalloped line indicates the position of the drytrough. Dashed boxes are the areas for which the National Severe Storms Forecast Center issued severe weather watches.

b. Relationship between 500-hPa thermal pattern and the CFA rainband

Seven 500-hPa charts were analyzed at 3-h intervals from 1800 UTC 8 March 1992 to 1200 UTC 9 March 1992. These analyses utilized rawinsondes launched from the standard National Weather Service (NWS) sites (at both synoptic and nonsynoptic times), as well as various additional sounding sites provided by the Storm Fronts and Experimental Systems Test (STORM-FEST). We show two maps from this series, which illustrate the results of the analysis and the data available at nonstandard (Fig. 4a, 2100 UTC 8 March) and standard (Fig. 4b, 1200 UTC 9 March) launch times. In all seven maps it was possible to follow consistently the leading edge of cold-air advection aloft (the dashed line in Fig. 4) as a cold baroclinic zone and an associated short-wave trough moved eastward. Notice that the baroclinic zone did not become appreciably stronger during this period, and the gradient of dewpoint at 1200 UTC 9 March (Fig. 4b) exceeds the temperature gradient behind the leading edge of cold-air advection; therefore, the change in humidity was the strongest indicator of the push of cooler and dryer air aloft. Temperature analyses at lower-tropospheric levels (not shown) show that the cold-air advection did not reach the surface; therefore, following Hobbs et al. (1990), we will refer to the leading edge of the cold-air advection as cold frontogenesis aloft (or CFA).

The positions of the CFA at 500 hPa, the drytrough, and the low-pressure center at the surface, together with radar echoes (from the digitized NWS radars) and the IR satellite depiction at 3-h intervals from 1800 UTC 8 March to 0900 UTC 9 March, are shown in Fig. 5. The surface position of the drytrough was derived from analyses of the surface data. Digitized radar data were available only within the white box shown in Fig. 5. A precipitation feature, identified as the pre-drytrough rainband by Martin et al. (1995), is indicated in Fig. 5 by dark gray shading (black shading is used for all other radar returns).

It can be seen from Fig. 5a that there were no cloud or radar echoes along the drytrough at 1800 UTC 8 March. However, as the CFA approached the drytrough (Fig. 5b), a few radar echoes and high clouds appeared in north-central Texas, south of the Red River. As the CFA at 500 hPa passed over the drytrough at 0000 UTC 9 March (Fig. 5c), further radar echoes and high cloud developed along the drytrough. By 0300 UTC 9 March substantial radar echoes filled the region between the CFA and the drytrough, in addition to a large radar echo ahead of the CFA on the Arkansas–Oklahoma border (Fig. 5d). The clouds along the southern portion of the drytrough indicate that precipitation occurred between the CFA and the drytrough as far south as southern Texas. By 0600 UTC the radar echoes had taken on the shape of a rainband stretching from southern Nebraska to northern Texas (Fig. 5e), and digitized NWS radar data show that the precipitation extended into southern Texas. By this time the rainband had moved away from the drytrough and was clearly aligned along the CFA. By 0900 UTC 9 March, the rainband was coincident with the CFA as it continued to move eastward away from the drytrough (Fig. 5f). The clear connection between the positions of the CFA and the squall line is the reason why we refer to this precipitation feature as the CFA rainband.

The pattern of higher-level clouds associated with the CFA rainband, as depicted by the IR satellite data, indicates that this rainband was associated with strong convection and with an anvil that spread out east of the precipitation. The radar data and surface reports confirm these inferences. Figure 6 shows the radar reflectivity pattern at 0743 UTC 9 March from the NCAR CP-4 Doppler radar, which was located in the northeast corner of Kansas. The dominant feature is a narrow convective line of strong reflectivity (50 dBZ), followed by a more uniform zone of weaker echoes. This reflectivity pattern is typical of a squall line (Smull and Houze 1985). Severe weather was associated with the CFA rainband. An F1 tornado and 1-in.-size hail were reported at 0300 UTC 9 March in south-central Kansas. At 0500 UTC 9 March, more 1-in.-size hail and an F0

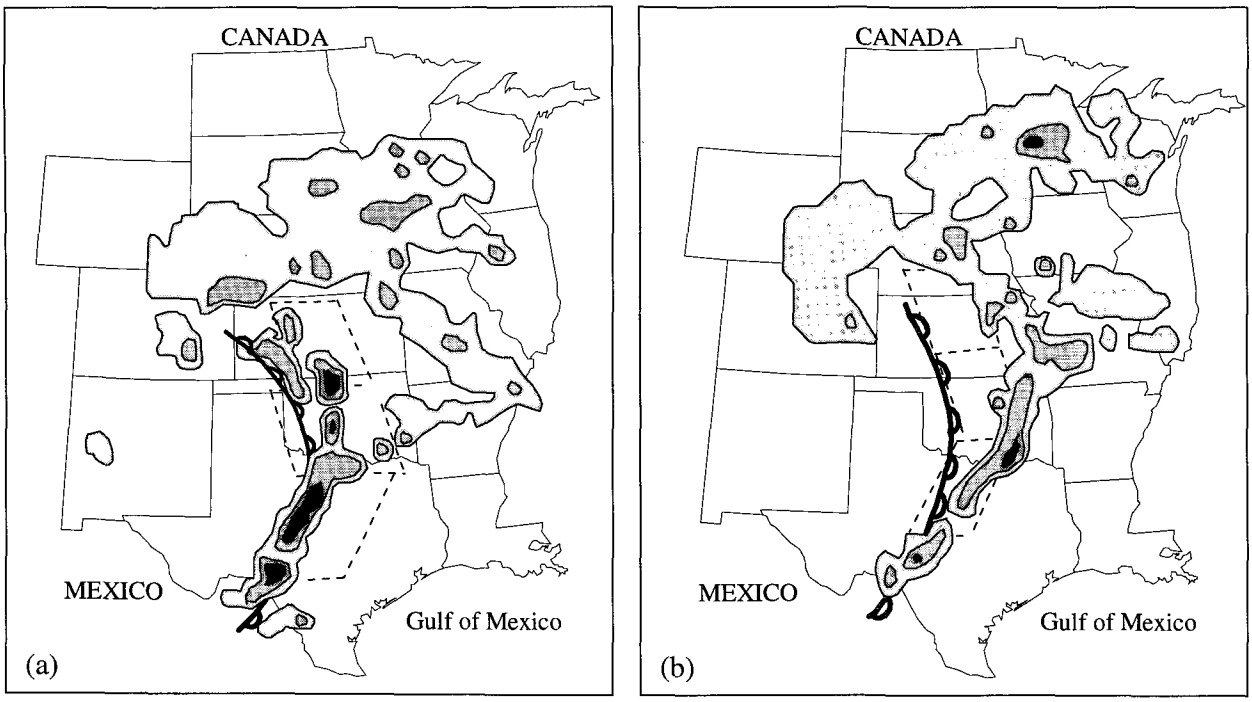

FIG. 3. (a) As for Fig. 2 except for 0235 UTC 9 March 1992. (b) As for Fig. 2 except for 0635 UTC 9 March 1992.

tornado were reported in southeastern Kansas. Farther south in Oklahoma, softball-size hail was reported at 0400 UTC 9 March. As the CFA rainband passed over Topeka, Kansas (TOP), and Kansas City, Missouri (MCI), both stations reported cloud-to-cloud and cloud-to-ground lighting. Reports of severe weather and regular station observations indicated that the CFA rainband decreased in convective intensity and areal coverage as it passed into Missouri and Arkansas. The NWS radar summaries (Figs. 3a,b) and the more detailed NWS digitized radar depictions (Figs. 5d–f) indicate that the CFA rainband was not continuous along its length but divided into several smaller segments. The even more detailed radar observations from the NCAR CP-4 Doppler radar (Fig. 6) show that the large segment of the CFA (Fig. 5e) that stretched from the Kansas–Oklahoma border into southern Nebraska was composed of even smaller segments. Each such segment of the CFA was characterized by a line of fairly continuous cumulonimbus clouds. Based on these radar observations and the surface station reports, we conclude the CFA rainband was most likely composed of multiple distinct lines of severe convection that resembled squall lines.

c. *Model simulations and the vertical structure of the CFA*

The evolution and vertical structure of the CFA was investigated using the Penn State–NCAR MM4 model (Anthes and Warner 1978; Anthes et al. 1987). The version of the model we used included a high-resolution planetary boundary layer (Blackadar 1979; Zhang and Anthes 1982) and prognostic equations for water vapor, cloud water, and rainwater. The terrain was represented by actual heights on a 0.5° × 0.5° latitude–longitude grid. The domain contained 61 × 61 grid points with a grid size of 45 km centered at 40°N, 96°W. The model atmosphere was divided into 23 layers from the surface to 50 hPa, and a sigma vertical coordinate system was used. The model was initialized using National Meteorological Center (NMC) gridded data as a "first guess" field, supplemented by NMC and global operational surface and rawinsonde data, and snow cover and land-use data prepared and maintained by NCAR. The lateral boundary conditions were linearly interpolated in time using observational data at 12-h intervals.

The model accurately reproduced the structure and movement of the CFA and the drytrough over a model run from 1200 UTC 8 March to 1200 UTC 9 March. Figure 7 shows the model 500-hPa geopotential height and temperature fields at 0300 UTC 9 March. These fields are very good simulations of the actual fields, some examples of which are shown in Fig. 4. A more detailed comparison of the model results with real data is given by Martin et al. (1995).

Figure 8 shows successive positions of the CFA at 500 hPa derived from the MM4 model outputs and the surface positions of the drytrough derived from obser-

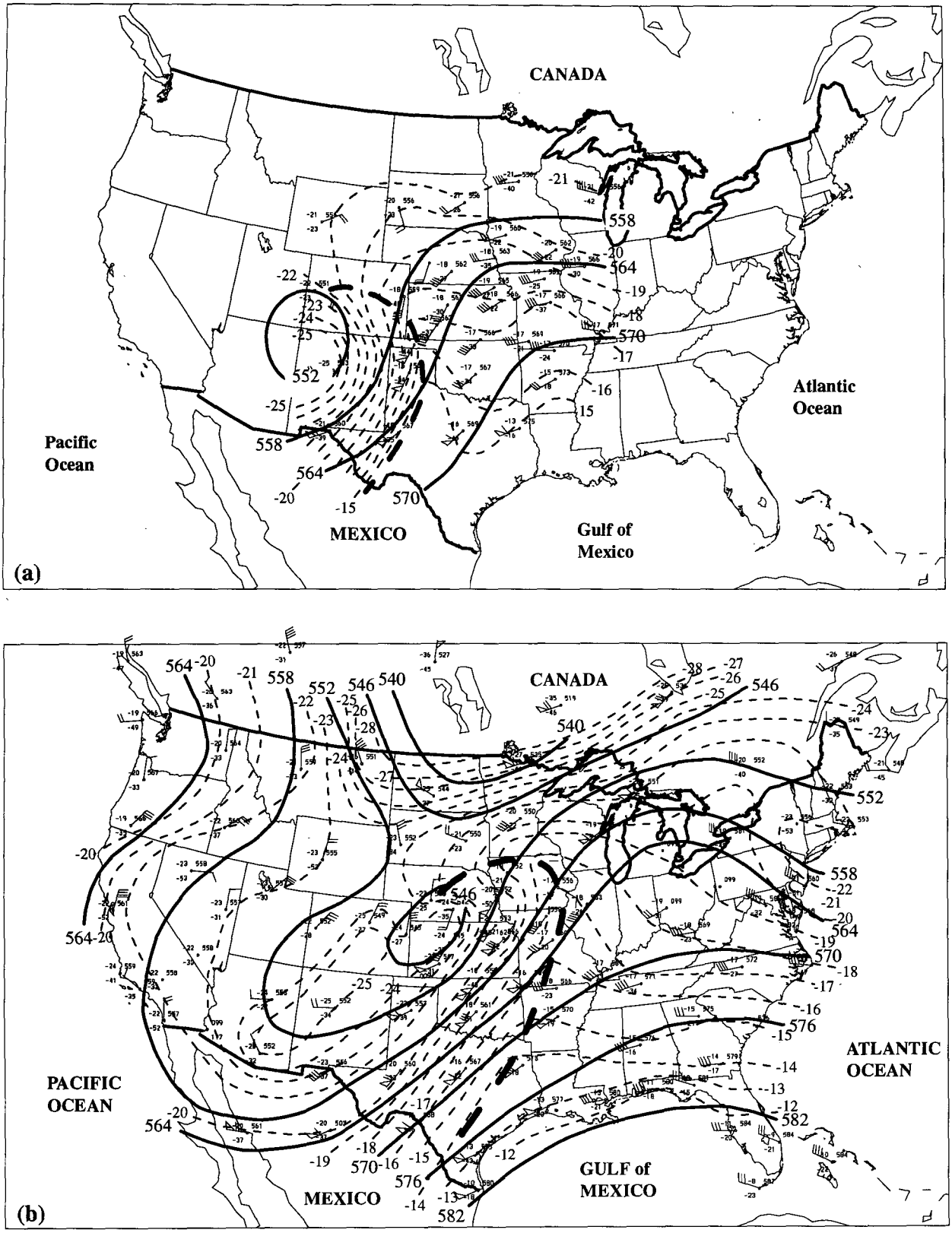

FIG. 4. (a) As for Fig. 1a but at 2100 UTC 8 March 1992. Isotherms are contoured every 1°C.
(b) As for Fig. 1a but at 1200 UTC 9 March 1992.

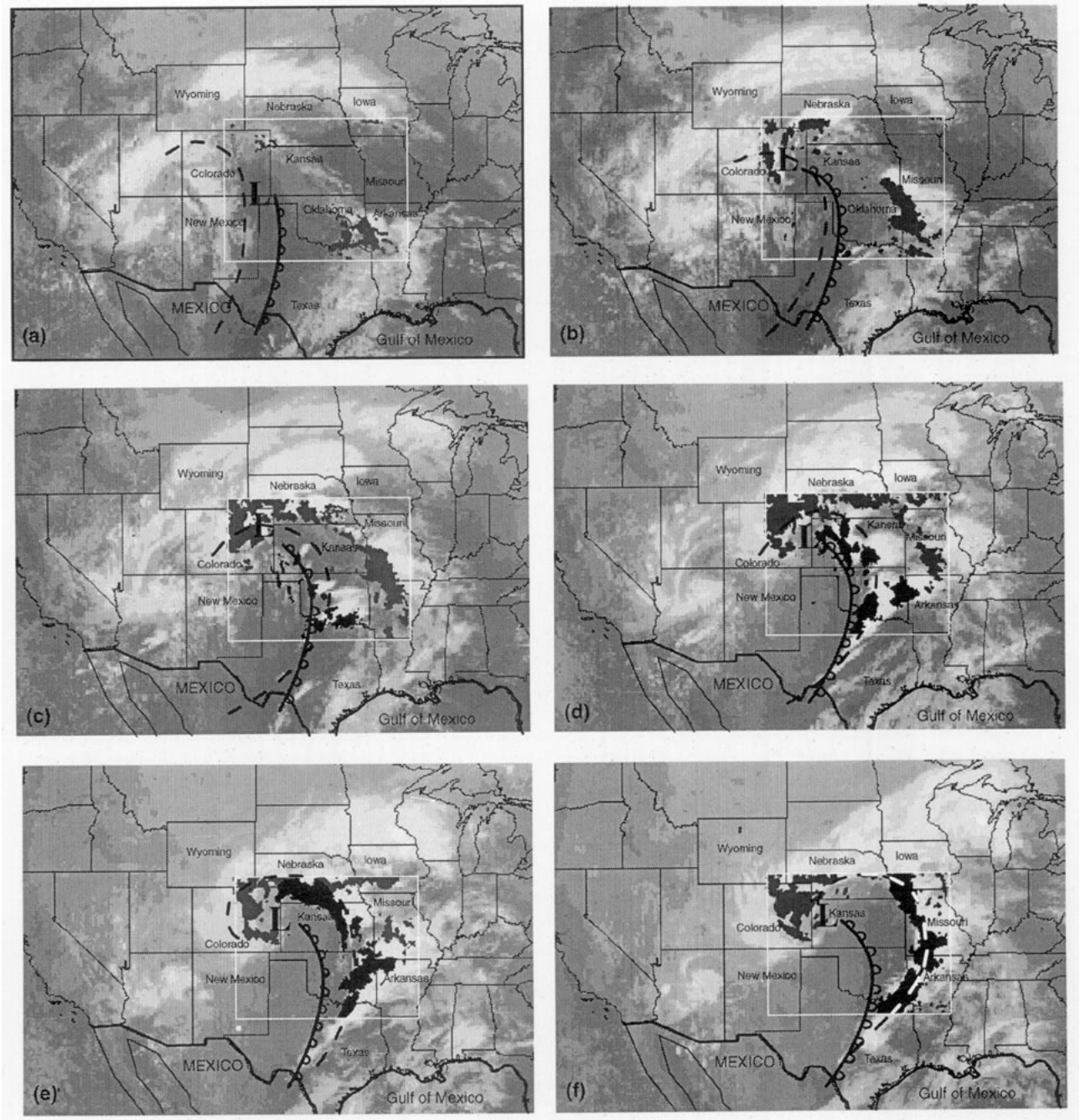

FIG. 5. National Weather Service digitized radar echoes (dark gray and black shading), shown within the white box only, superimposed on IR satellite imagery (white shading) at (a) 1800 UTC 8 March 1992, (b) 2100 UTC 8 March 1992, (c) 0000 UTC 9 March 1992, (d) 0300 UTC 9 March 1992, (e) 0600 UTC 9 March 1992, and (f) 0900 UTC 9 March 1992. Also shown are the CFA at 500 hPa (heavy dashed line), the surface positions of the drytrough (heavy scalloped line) and the low pressure center (L), and the pre-drytrough rainband (radar echoes with dark gray shading).

vations. A time sequence of cross sections (derived from the MM4 model outputs) of temperature, potential temperature, and the positions of the CFA and the drytrough along line AA' in Fig. 8 are shown in Fig. 9. The positions of the CFA on these sections were determined from the locations of the leading edge of cold-air advection on constant pressure maps at various pressures. However, there is also a good correspondence between the positions of the CFA and the leading edge of the temperature decrease.

Martin et al. (1995) showed that the drytrough in this case had a warm frontal–like circulation to its east.

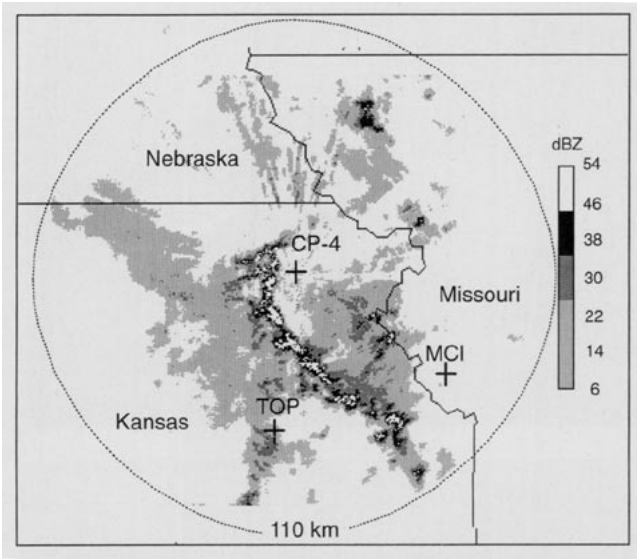

FIG. 6. Radar echoes at 0743 UTC 9 March 1992 from the NCAR CP-4 radar at 0.4° elevation.

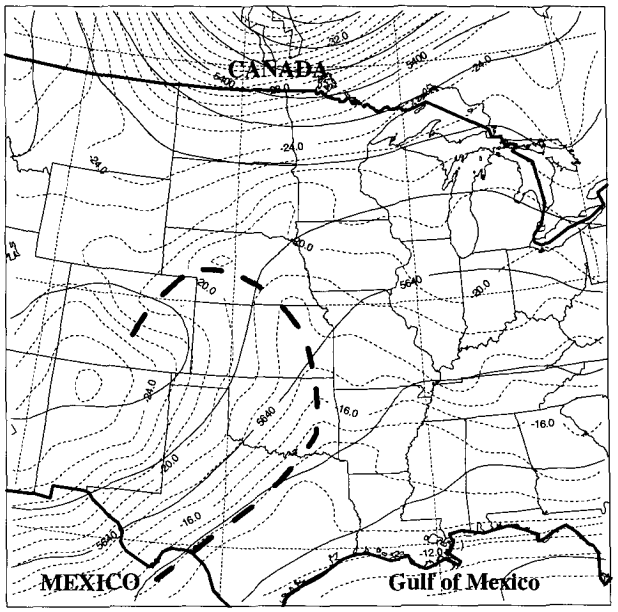

FIG. 7. 500-hPa map at 0300 UTC 9 March from MM4 model 15-h forecast. Solid lines are geopotential height (m) and dashed lines are isotherms (°C, contoured every 1°C). The CFA at 500 hPa is shown by the heavy dashed line.

This circulation created an upward-sloping layer of potentially unstable stratification. Figure 10 shows the progression of the potentially unstable layer (θ_e decreasing with height) from 1200 UTC 8 March to 0000 UTC 9 March in a vertical cross section along line *BB'* in Fig. 8.

As the CFA advanced eastward from the Rockies over the Great Plains, three important simultaneous changes occurred in the structure of the atmosphere. (These changes can be seen in Fig. 8, the four panels of Fig. 9, and the three panels of Fig. 10.) First, as the nose of the CFA moved eastward over the drytrough, the CFA began to tip forward. Second, at the same time, the potentially unstable layer of air associated with the circulation of the drytrough continued to thrust upward and eastward, away from the surface position of the drytrough. This sloped lifting of the potentially unstable layer by the circulation associated with the drytrough helped to bring the potentially unstable layer closer to saturation and therefore closer to realizing the instability inherent in the stratification. Third, as the drytrough moved eastward, down the slope of the Great Plains, the cold air at low levels to the west of the CFA moved into the position of the drytrough. Downslope flow and adiabatic warming removed much of the temperature difference at the surface between the warm air east of the drytrough and the sinking cold air (Martin et al. 1995). This can be seen in the development of the low-level axis of warm air over the drytrough (Figs. 9a–d). Although there was a *temperature* gradient on the surface west of the drytrough, there was only a slight *potential temperature* gradient in this region. This suggests that the temperature gradient was simply a manifestation of the sloping topography. However, above the surface, a temperature gradient is apparent west of the CFA. As the CFA moved over the underlying region of warm-air advection and the upward-sloping zone of potentially unstable air (see the axis of warm temperatures ahead of the CFA in Figs. 9a and 9b), a warm occluded-like structure formed. Here, the

FIG. 8. Surface positions of the drytrough (scalloped lines with times in UTC), and the positions of the CFA (dashed lines) at 500 hPa from MM4 model simulations.

drytrough is analogous to a surface occluded front, and the CFA is analogous to an upper-level cold front. As this structure moved eastward, cooling occurred first aloft (with the CFA), while warming was continuing at lowers levels ahead of the drytrough. As in the case of a warm occluded front, the surface trough (drytrough) marks a wind shift and the transition from warming to cooling.

Interestingly, the surface temperature gradient west of the drytrough, which was produced by the sloping terrain, contributed to the misanalysis by the NWS of the drytrough as a cold front along the western slopes of the Great Plains.

The shaded regions in Fig. 9 show the location of upward air motion within the cold air derived from the MM4 model. The primary area of upward motion occurred where the advancing cold air was riding over the general lifting in the warm-air advection east of the drytrough. This lifting was responsible for the changing shape of the CFA. Model results indicated that the adiabatic cooling due to rising air dominated over horizontal temperature advection in determining the local temperature tendency in the portion of the cold air that moved over the surface drytrough and thus was instrumental in maintaining a distinct edge to the advancing cold air.

We have seen that the MM4 model simulations indicate that the lower atmosphere ahead of the advancing CFA was "primed" for severe weather by the circulation associated with the drytrough. To explain the outbreak of severe weather along the drytrough and between the drytrough and the CFA after it passed over the surface position of the drytrough, as well as the isolated outbreaks of convection ahead of the CFA, we will now discuss the thermodynamic conditions observed at the time of the outbreak of convection and trace the evolution of these conditions using both MM4 model simulations and observations.

3. Tropospheric destabilization east of the drytrough

a. Background

In order for severe convection to occur, such as that which characterized the CFA rainband in the case described here, tropospheric air must be lifted and become freely convective. The latter condition depends on the thermodynamic stratification of the atmosphere and its susceptibility to instabilities. The most potent form of instability is potential instability, which permits the formation of an absolutely unstable lapse rate (and therefore convective overturning) provided there is sufficient vertical lifting of the potentially unstable layer (e.g., Wallace and Hobbs 1977, 85–86).

Atmosphere conditions in the south-central United States on 8–9 March 1992 were ideal for the creation of extreme potential instability. The surface drytrough was characterized by a strong flow of warm moist air from the south at low levels, which was responsible for the northward transport (immediately east of the drytrough) of air from the Gulf of Mexico that had very high equivalent potential temperatures ($\theta_e > 330$ K). The southwesterly flow above 800 hPa was responsible for the placement of low-θ_e air (which originally resided over the high terrain of the southern Rockies and Mexican Plateau) over the low-level moist air. Thus, an axis of maximum potential instability (from the surface to 700 hPa) was created immediately east of the drytrough (Martin et al. 1995).

The sounding at Stephenville, Texas (SEP, location shown in Fig. 8), at 2100 UTC 8 March 1992 is shown in Fig. 11. A layer of uniform θ_e air extended from the ground to 720 hPa, and it was capped by a dry layer. Between 720 and 700 hPa the change in θ_e was 15 K, whereas the change in θ_e between the surface and 700 hPa was 20 K. Thus, 75% of the potential instability from the surface to 700 hPa was accounted for in the uppermost 20 hPa. The MM4 simulated sounding for Stephenville at this time shows a moist layer with nearly the same θ_e profile as the actual sounding but capped at 850 hPa. As a result, the potential instability was spread over a vertical interval of 150 hPa. This error in the moisture profile has a substantial effect on instability. For example, based on the actual Stephenville sounding at 2100 UTC 8 March, the layer from 720 to 700 hPa has to be lifted by only 20 hPa to create an absolutely unstable lapse rate and convective overturning. By contrast, this same amount of lifting is woefully insufficient to initiate convective motions in the MM4 model sounding.

In view of these considerations, we employed a combination of model outputs and measurements to explore how the atmosphere may have become destabilized in the hours (between 2100 UTC 8 March to 0000 UTC 9 March) leading up to the outbreak of convection along the drytrough. We will show that different processes were probably responsible for this destabilization in the northern and southern portions of the region where severe weather occurred.

b. Destabilization in the southern portion of the region of severe weather

Stephenville is a representative sounding site for investigating changes in atmospheric stability in the southern portion of the region in which severe weather occurred. The sounding at Stephenville for 1800 UTC 8 March (Fig. 12) shows a deep, surface-based, uniformly high θ_e layer extending up to 790 hPa. This layer was characterized by air with $\theta_e = 328$ K, and it was capped by a dry and almost isothermal layer (up to 700 hPa) in which θ_e was approximately 318 K. Thus, the layer from 800 to 750 hPa was intensely potentially unstable. In fact, lifting of the 800–750-hPa layer by just 40 hPa would have caused convective overturning.

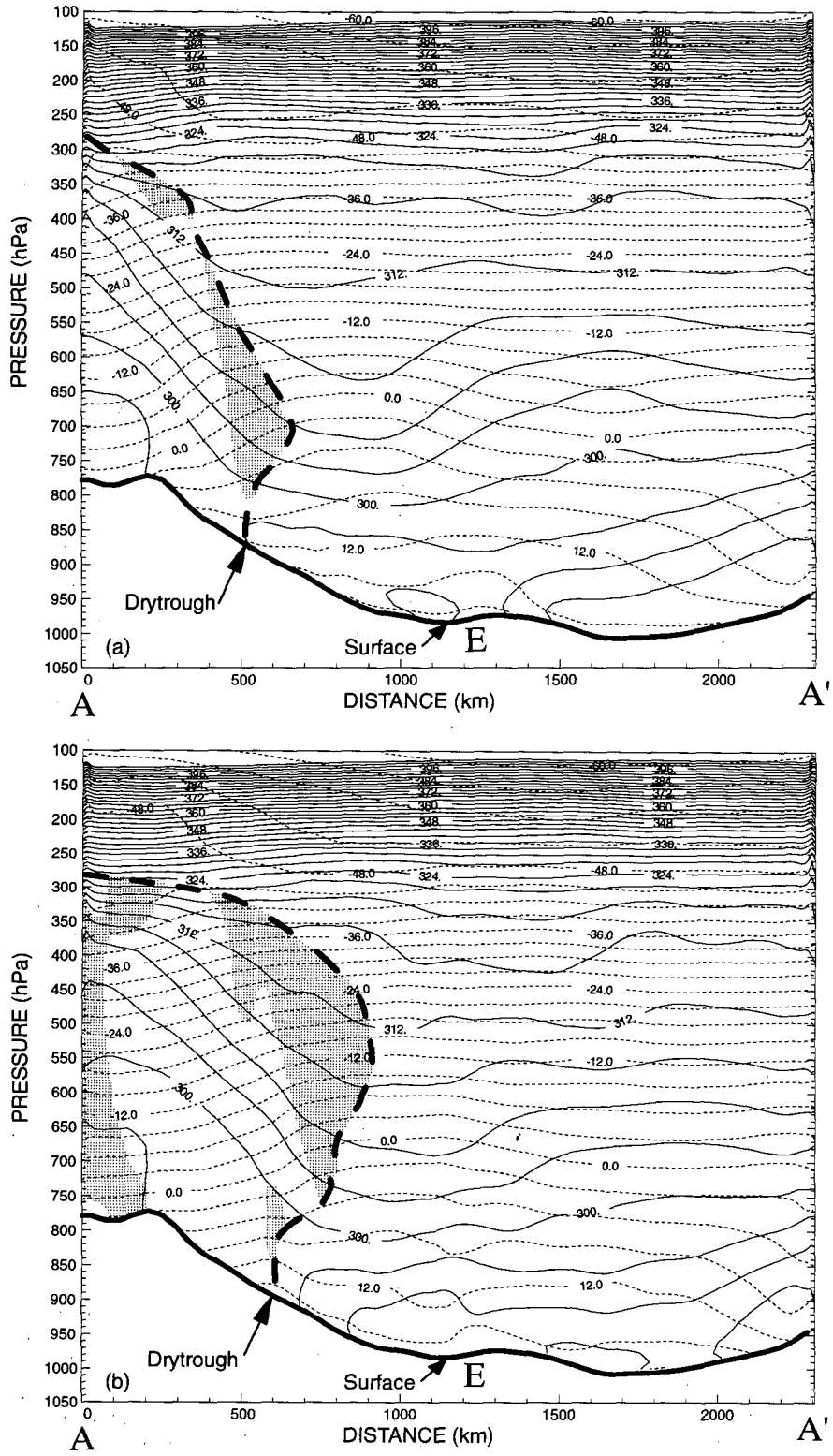

FIG. 9. Vertical cross sections along line *AA'* in Fig. 8 from MM4 model simulations showing potential temperature (K, contoured every 3 K), isotherms (°C, contoured every 3°C), position of the CFA (heavy dashed line), regions of upward vertical motion within the cold air (shaded), and the intersection (*E*) of the cross sections through lines *AA'* and *BB'* in Fig. 8 at (a) 1800 UTC 8 March 1992, (b) 0000 UTC March 9 1992, (c) 0600 UTC March 9 1992, and (d) 1200 UTC March 9 1992.

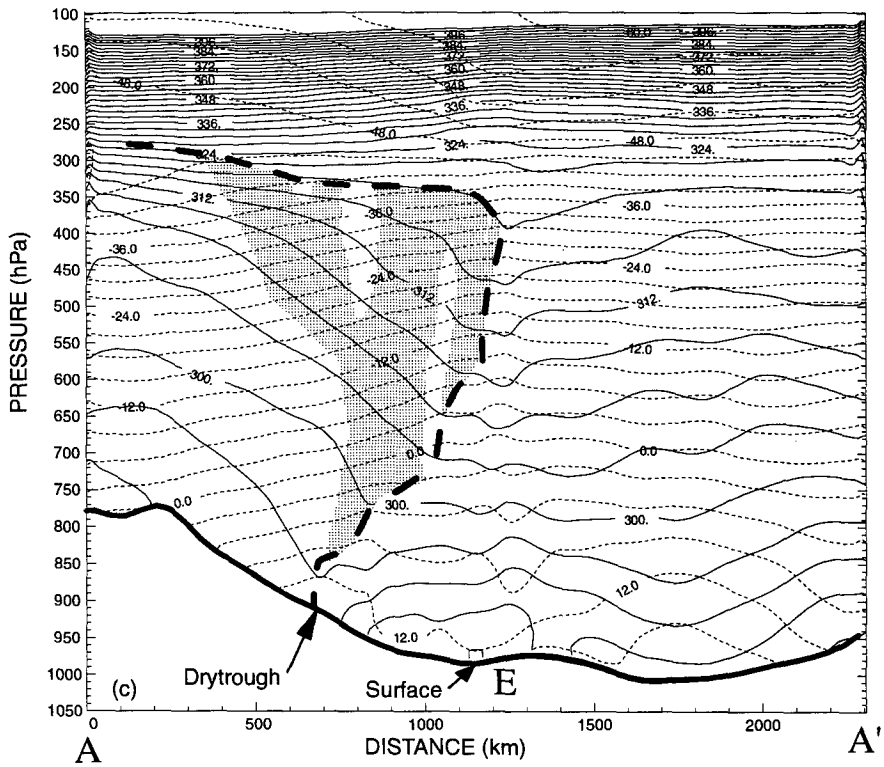

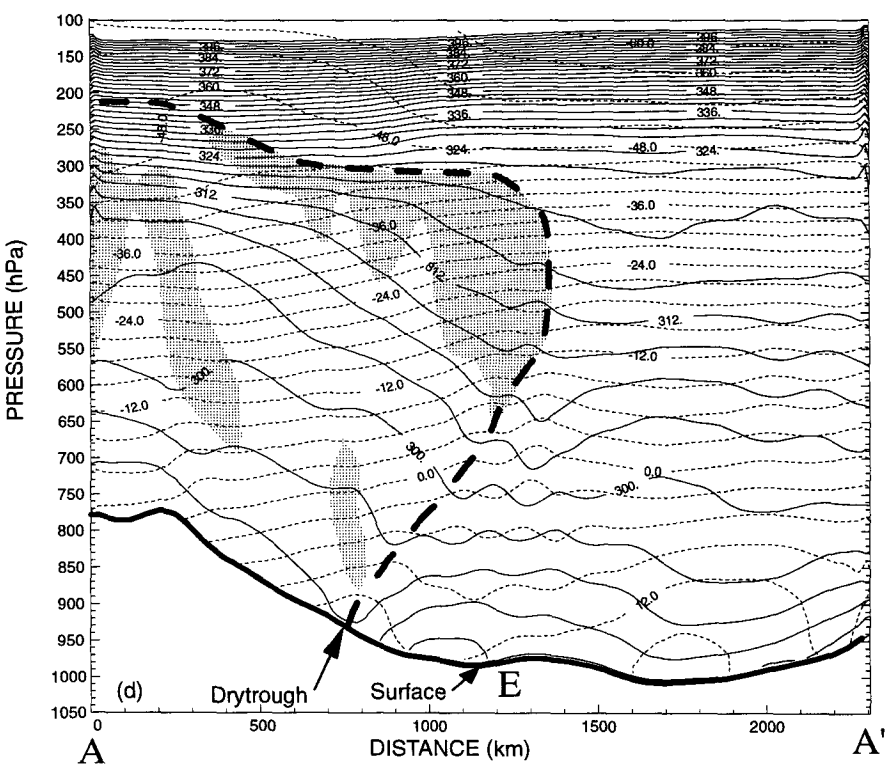

FIG. 9. (*Continued*)

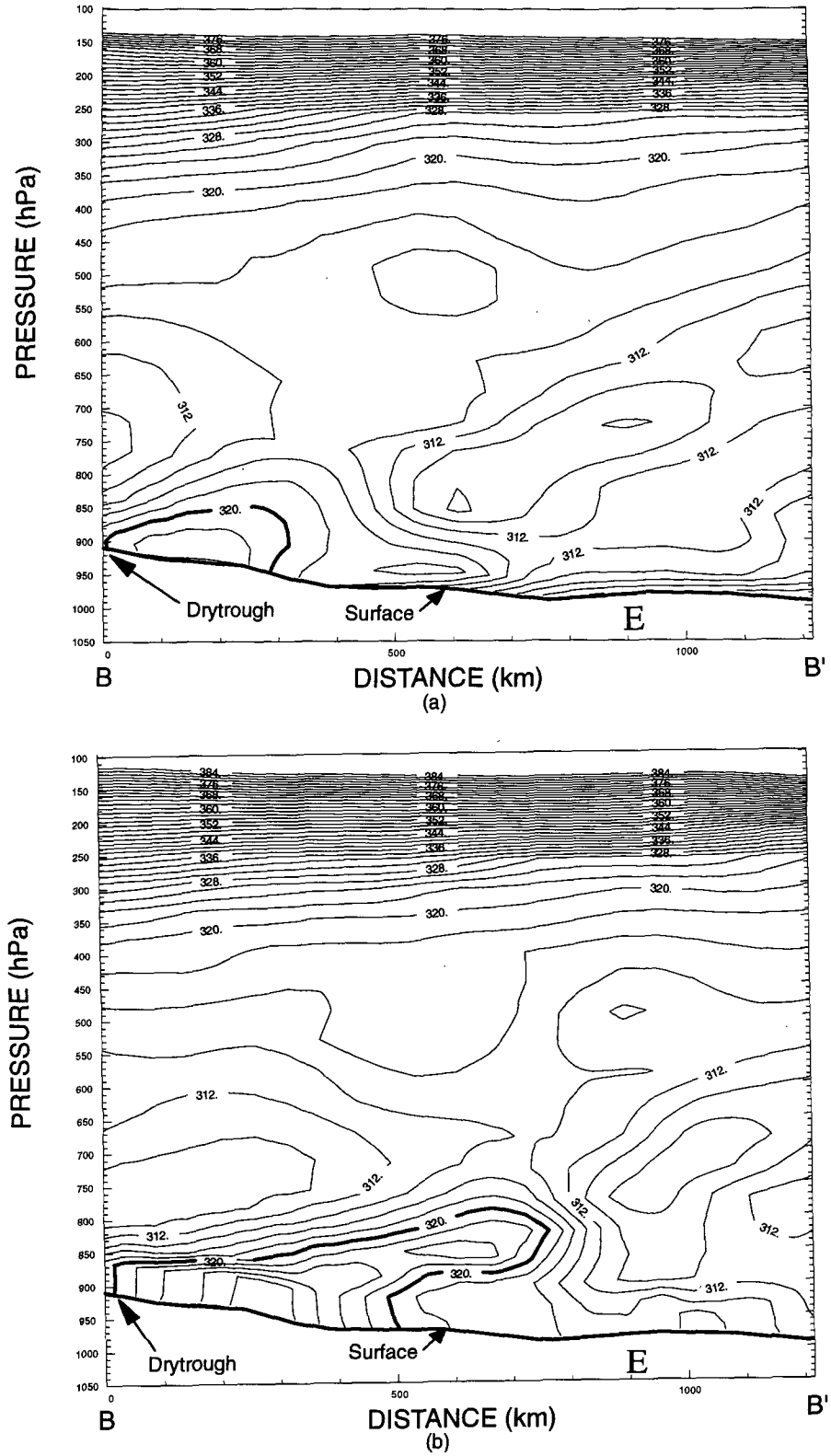

FIG. 10. Vertical cross sections along line *BB'* in Fig. 8 from the MM4 model simulations showing equivalent potential temperature (K, contoured every 2 K), the 320-K equivalent potential temperature line within the circulation of the drytrough (heavy line), and the intersection (*E*) of the cross sections through lines *AA'* and *BB'* in Fig. 8 at (a) 1200 UTC 8 March 1992, (b) 1800 UTC 8 March 1992, and (c) 0000 UTC 9 March 1992.

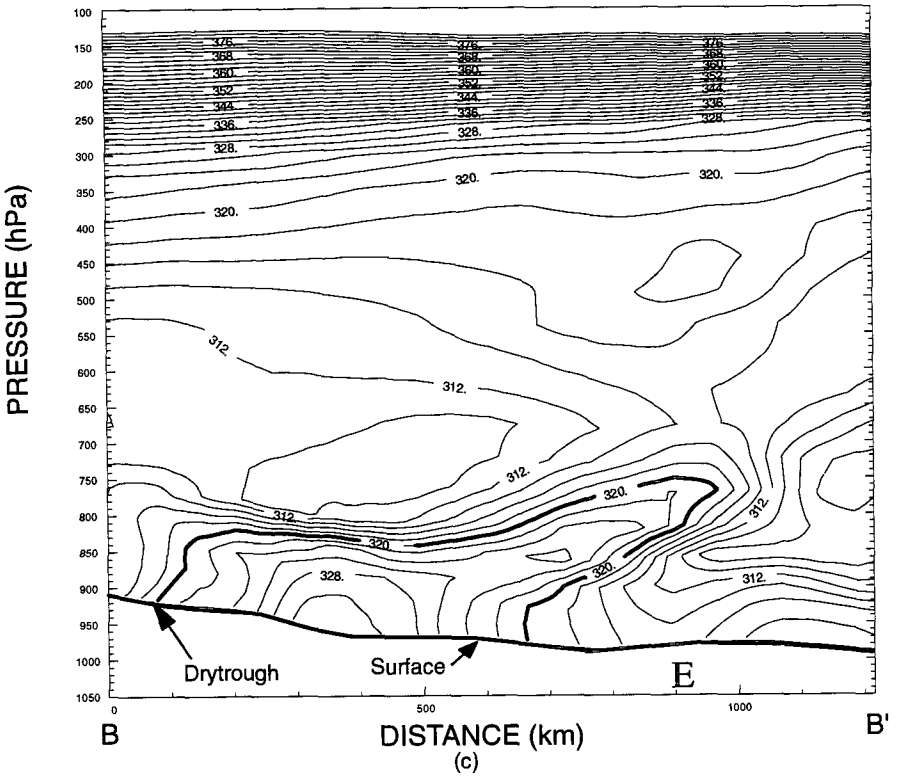

FIG. 10. (*Continued*)

However, the isothermal layer from 780 to 700 hPa placed a considerable cap on surface-based free convection. Therefore, despite the potential instability present in the sounding, it was not susceptible to deep convection.

By 2100 UTC the vertical stratification at Stephenville had changed considerably (see Fig. 11). The most notable changes were the depth of the uniform θ_e layer (from the surface to 720 hPa at 2100 UTC) and the absence of the capping isothermal layer atop the low-level moist air. The increased depth of the moist layer probably resulted from the circulation associated with the drytrough. Lifting would had to have been approximately 8 cm s^{-1} during the period from 1800 to 2100 UTC to account for the observed 70-hPa deepening of the moist layer. Further, if we assume that the capping isothermal layer was lifted by a similar amount over those three hours, then the capping isothermal layer from 780 to 700 hPa that was present at 1800 UTC would have been erased by 2100 UTC as a result of differential adiabatic cooling.

To check the plausibility of this scenario, we compared MM4 model-generated soundings for Stephenville at 1800 and 2100 UTC. Although these soundings were very inaccurate with respect to the moisture content of the atmosphere, the layer from 650 to 750 hPa cooled by 1°C between 1800 and 2100 UTC in the model simulation. Based on the instantaneous MM4 model-simulated values at 1800 UTC, horizontal warm-air advection in this layer was about 4.2°C (3 h)$^{-1}$. Therefore, assuming that the flow was dry adiabatic (a good assumption since no convection was reported at Stephenville until nearly 0000 UTC 9 March), the net local cooling predicted by the MM4 model at Stephenville was due to horizontal warm-air advection offset by an adiabatic temperature change produced by vertical motions.

The magnitude of the vertical motions required to offset the temperature rises due to the warm-air advection is roughly 10 cm s^{-1}, which is very similar to the value deduced (in a cruder fashion) from consideration of the observed increase in depth of the moist layer in the Stephenville sounding between 1800 and 2100 UTC 8 March. Lifting on the order of 10 cm s^{-1} operating on the extreme instability of the 720–700-hPa layer in the 2100 UTC Stephenville sounding would quickly manifest itself in severe convection, which, in fact, occurred by about 2230 UTC 8 March 1992. We conclude that in the southern portion of the region in which severe weather occurred (Texas), the atmosphere was destabilized by modest synoptic-scale vertical velocities and associated adiabatic cooling, and this removed the capping isothermal layer that had previously inhibited the development of deep convection.

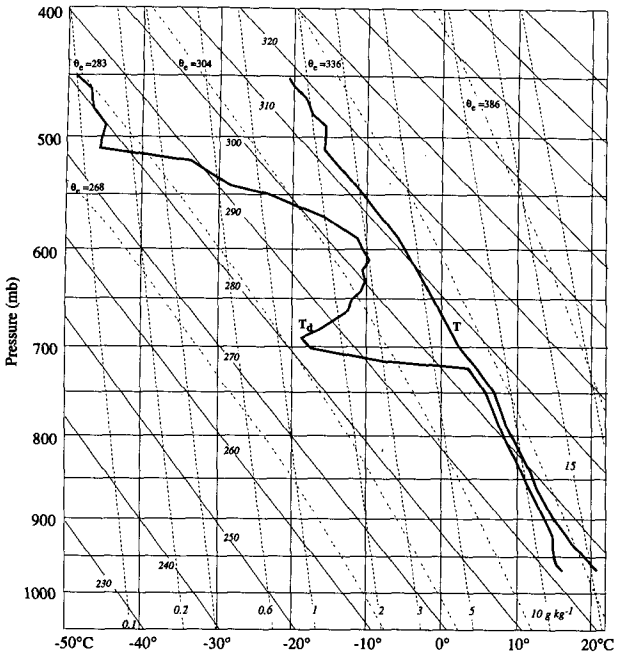

FIG. 11. Sounding for Stephenville, Texas (SEP), at 2100 UTC 8 March 1992. Temperature and dewpoint are plotted on a pseudoadiabatic diagram. Vertical solid lines are isotherms (°C). Sloping solid lines are isentropes (K). Single dashed lines are constant saturation mixing ratios (g kg^{-1}). Double-dashed lines are pseudoadiabats [labeled in equivalent potential temperature (K)].

c. *Destabilization in the northern portion of the region of severe weather*

Dodge City, Kansas (DDC, location shown in Fig. 8), is a representative sounding for diagnosing the destabilization in the northern portion of the region (Oklahoma and Kansas) in which severe weather occurred. At 1800 UTC 8 March 1992, the sounding at DDC was characterized by a fairly well mixed unsaturated layer of θ_e = 322 K, which extended from the surface (910 hPa) to 770 hPa (Fig. 13a). Directly atop this layer, from 770 to 750 hPa, was a 2°C temperature inversion. This inversion was coincident with a considerable decrease in moisture content. Potential instability was fairly large at the interface between the moist layer below and the dry layer aloft, but it was restrained from being released by the presence of the inversion.

By 2100 UTC the mixed layer of high-θ_e air had deepened by 70 hPa to 700 hPa, but it was still capped by a significant inversion (Fig. 13b). The inversion explains the lack of convective activity in the vicinity of Dodge City at this time. Between 2100 and 0000 UTC 9 March, this inversion was erased and replaced by a layer of less, but still large, static stability from 680 to 630 hPa (Fig. 13c). The top of the moist layer rose 30 hPa, from 700 to 670 hPa, during this time period. Concurrently, there was modest cold-air advection at and near the 650-hPa level. The MM4 model simulation indicated that this advection produced a cooling rate of (about) 2.8°C (3 h)$^{-1}$ (at the level of maximum cold-air advection, 660 hPa). This cooling was not sufficient to explain the observed 4°C (3 h)$^{-1}$ temperature change in the 700–620-hPa layer that erased the inversion at Dodge City. Assuming, again, that the rise of the top of the moist layer is evidence of a general lifting of a similar magnitude throughout the lower troposphere, then a combination of modest cold-air advection and lifting of the column between 750 and 650 hPa by 30 hPa (~3 cm s^{-1}), between 2100 UTC 8 March and 0000 UTC 9 March, would have resulted in the observed removal of the capping inversion at Dodge City during that period. Thus, a combination of weak synoptic-scale lifting and midlevel cold-air advection probably acted to destabilize the soundings in the northern portion of the region of severe weather. Since the CFA moved through Dodge City between 1800 UTC 8 March and 0000 UTC 9 March, we attribute the cold-air advection to the midlevel baroclinic zone associated with CFA and the lifting of the air to the circulations associated with the drytrough and cold frontogenesis aloft. These processes could have caused the general outbreak of convection between the drytrough and the CFA as the latter moved east of the drytrough.

4. Mechanisms for the formation of the CFA rainband

The coincidence of the CFA and the CFA rainband after 0300 UTC 9 March (Fig. 5) indicates their strong

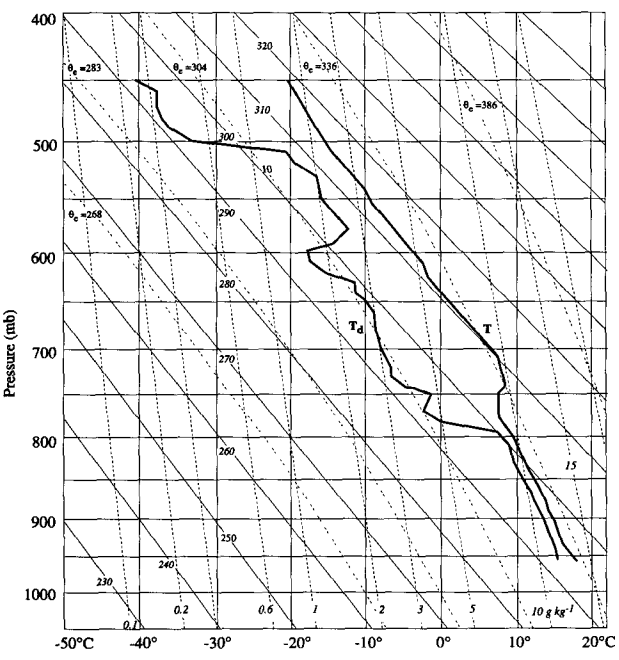

FIG. 12. As for Fig. 11 but for 1800 UTC 8 March 1992.

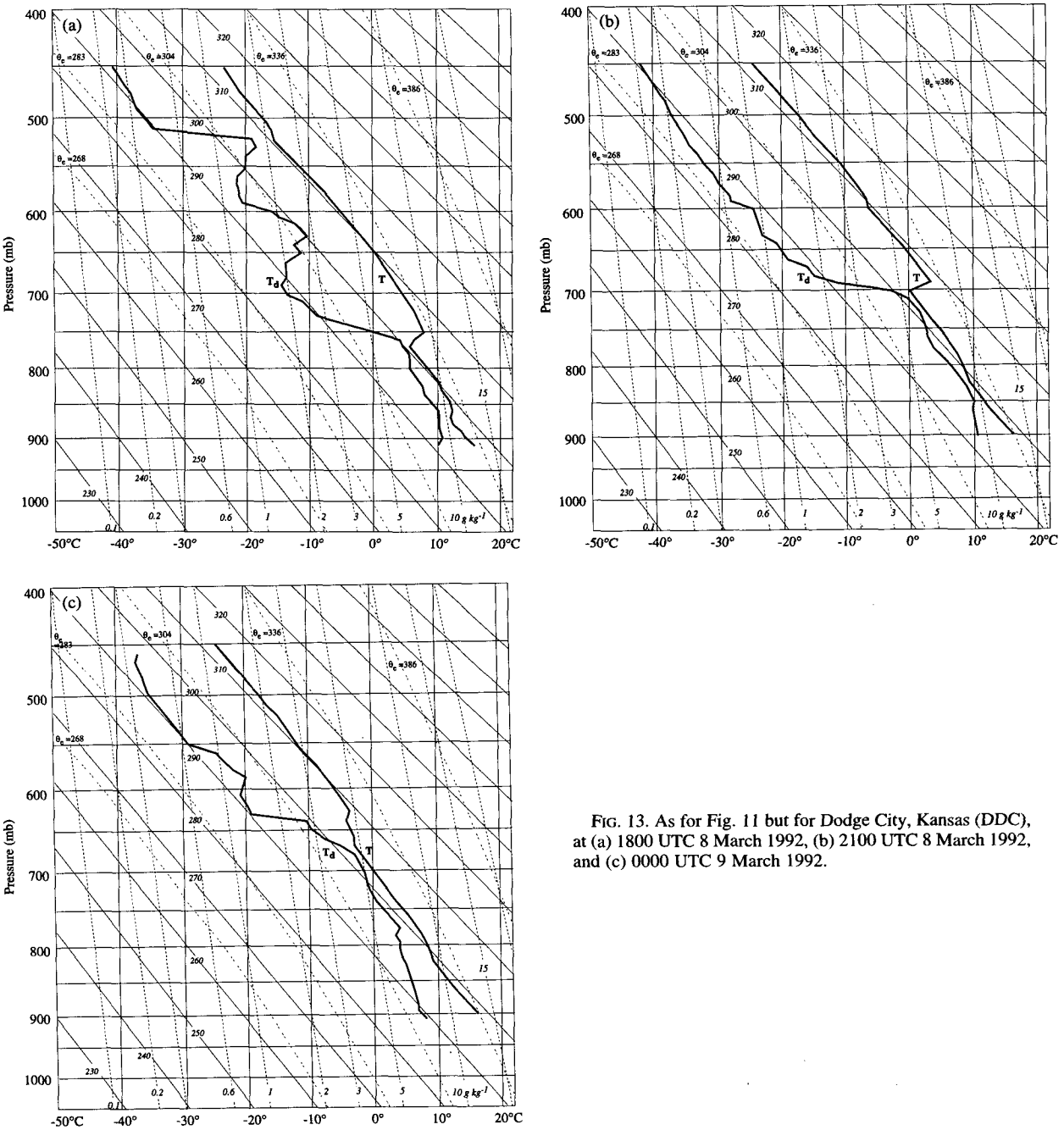

FIG. 13. As for Fig. 11 but for Dodge City, Kansas (DDC), at (a) 1800 UTC 8 March 1992, (b) 2100 UTC 8 March 1992, and (c) 0000 UTC 9 March 1992.

connection. In this section we will show that two processes contributed to the formation of the CFA rainband: frontogenesis (where quasigeostrophic theory applies) and a change in the horizontal pressure gradient under the nose of the advancing cold-air advection aloft (where quasigeostrophic theory does not apply).

a. Quasigeostrophic frontogenesis

The first process (frontogenesis) can be diagnosed using quasigeostrophic dynamics. The CFA represents a boundary between cold-air advection to the west and warm-air advection to the east. Such a region of differential horizontal temperature advection is likely to be accompanied by a thermally direct vertical circulation. Evidence for such a circulation can be obtained by using the Q vector to diagnose the synoptic-scale environment in which the CFA rainband developed, where convergence (divergence) of $\mathbf{Q}$ implies upward (downward) vertical motion (Hoskins et al. 1978). Here $\mathbf{Q}$ is defined as

$$\mathbf{Q} = \left(\frac{-\partial \mathbf{V}_g}{\partial x} \cdot \nabla\theta \mathbf{i}, \frac{-\partial \mathbf{V}_g}{\partial y} \cdot \nabla\theta \mathbf{j} \right). \quad (1)$$

The Q vector can be used also to determine the quasigeostrophic frontogenesis function F (i.e., the Lagrangian rate of change of $|\nabla\theta|$ following the geostrophic flow) from the following expression:

$$F = \frac{1}{|\nabla\theta|} (\mathbf{Q} \cdot \nabla\theta). \quad (2)$$

In regions where the Q vectors are directed across the isotherms from cold to warm air there is frontogenesis, which will be accompanied by a thermally direct vertical circulation. Figure 14a shows the Q-vector convergence at 500 hPa at 2100 UTC 8 March calculated from the MM4 model (2100 UTC was chosen as a representative time; similar patterns were observed at other times). The Q-vector convergence located in south-central Colorado is related to the development of the surface low pressure center. The region of Q-vector convergence stretching from the eastern Texas panhandle toward the Rio Grande is associated with the CFA. This region is coincident with the axis of maximum potential instability and the outbreak of severe convection along and to the east of the drytrough.

Values of F at 500 hPa at 2100 UTC 8 March are shown in Fig. 14b. An axis of frontogenesis, associated with the CFA, stretches from the Texas panhandle to the Rio Grande. The thermally direct vertical circulation that must be associated with this frontogenetic region is exactly that implied by the divergence of $\mathbf{Q}$ shown in Fig. 14a. As the CFA propagated eastward, it maintained its frontogenetic characteristics and therefore remained the seat of a thermally direct vertical circulation coincident with the CFA rainband.

As pointed out by Sanders and Hoskins (1990), quasigeostrophic theory can be used with confidence to describe only the broad aspects of the vertical motion field, not mesoscale details. The CFA rainband was a mesoscale feature with a very narrow width (Fig. 6). The mesoscale nature of this rainband can be explained in part by the fact that synoptic-scale forcing was superimposed on a region of mesoscale potential instability. Such conditions can produce narrow bands of precipitation within broad frontal zones (Sanders and Bosart 1985; Moore and Blakely 1988; Martin et al. 1992).

b. *Cold-air advection*

In the region of upward motion associated with the CFA, the leading edge of cold-air advection may have acted to enhance the vertical motion below the nose of the cold air. This is the second process that contributed to the formation of the CFA rainband.

Figure 15 shows the magnitude of the surface pressure gradient at 0300 UTC 9 March and the positions of the surface drytrough and the CFA at 500 hPa. Surface observations indicate that the pressure was falling

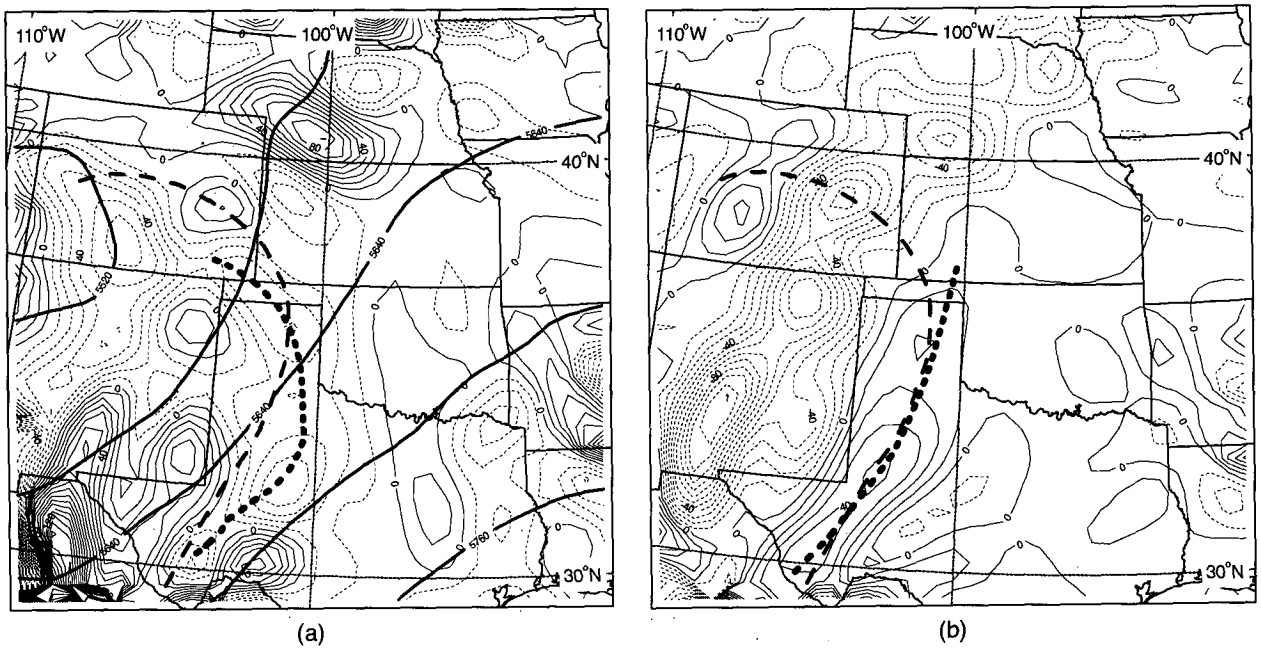

(a) (b)

FIG. 14. (a) Q-vector convergence at 500 hPa at 2100 UTC 8 March 1992 (10^{-16} K m^{-2} s^{-2}). Also shown are geopotential heights (m, contoured every 30 m; heavy solid). The heavy dotted line is the axis of Q-vector convergence associated with the CFA. The heavy dashed line is the position of the CFA at 500 hPa. (b) Quasigeostrophic frontogenesis (10^{-11} K m^{-1} s^{-1}) at 500 hPa at 2100 UTC 8 March 1992. The heavy dotted line is the axis of frontogenesis associated with the CFA, and the heavy dashed line is the position of the CFA at 500 hPa.

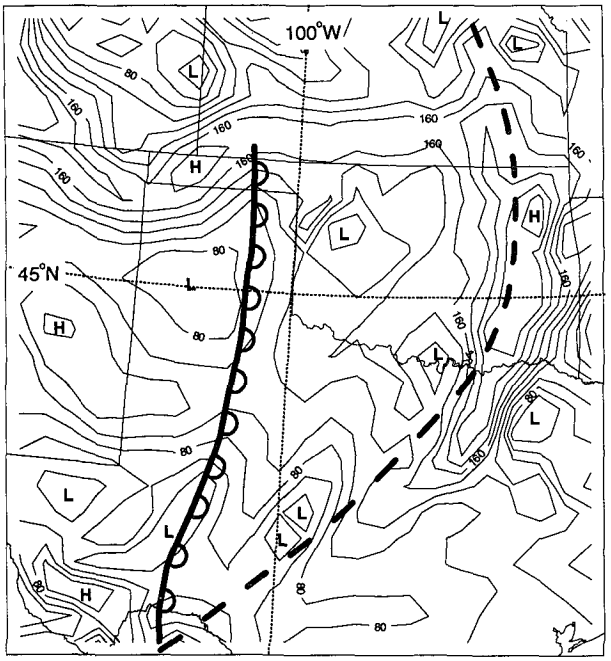

FIG. 15. Magnitude of the surface pressure gradient (10^{-7} hPa m^{-1}, contoured every 20 × 10^{-7} hPa m^{-1}) predicted by the MM4 model simulations at 0300 UTC 9 March 1992. The heavy dashed line is the 500-hPa position of the CFA, and the surface position of the drytrough is indicated by the scalloped line.

everywhere east of the drytrough. Accordingly, based on the pattern shown in Fig. 15, a surface station would have experienced an increase in the rate of fall of pressure as the CFA approached and then a decrease in the rate of fall of pressure as the CFA passed overhead. Coincident with this change in the rate of pressure fall at the surface was surface convergence (Fig. 16) and related upward vertical motion at 850 hPa (Fig. 17). The convergence and upward vertical velocity associated with the CFA were distinct from the convergence and upward vertical velocity aligned with the drytrough farther west.

Figures 4 and 9 show that the passage of the CFA was accompanied by a gradual warming of the atmosphere ahead of the CFA and subsequently more rapid cooling of the portion of the atmosphere behind the CFA. This warming–cooling couplet could account (hydrostatically) for the change in the rate of pressure fall at the surface that was coincident with the passage of the CFA and the related convergence and upward air motion beneath the nose of the CFA.

The rapid change in the pressure gradient beneath the nose of the CFA would have produced convergence in the following manner. Since the CFA moves relative to air parcels beneath its nose, parcels that are in geostrophic balance (excluding friction) will have to (geostrophically) adjust to the rapidly changing pressure gradient associated with the migrating CFA. It is this adjustment that leads to convergence and upward motion of air. Since the time period for this adjustment is about 1 h, geostrophic balance is never attained for such parcels. Indeed, the rate of change of the pressure gradient is fast enough that the equations for the isallobaric wind (which assume that the component of the wind along the isobars is always in geostrophic balance with the changing gradient) do not apply.

To test this hypothesis we did a 2D numerical calculation. The grid was 20 km × 11 km, with a 50-km horizontal resolution and 1-km vertical resolution. We assumed a constant speed for the CFA of 10 m s^{-1} (derived from Fig. 9) and a time step of 5000 s. The calculation was based on temperature data produced by the MM4 model simulation valid at 0300 UTC 9 March 1992 at and above 5 km in the region where the cold-air advection was initiated; below 5 km a constant horizontal temperature field was used. From the initial temperature distribution we obtained the pressure field by downward integration of the hydrostatic equation. As a boundary condition, we assumed that at the top of the grid (10 km) the pressure had a constant value of approximately 264 hPa. Although the assumption of a constant value of pressure at 10 km is unrealistic, it allows determination of the nature of the signal generated on the surface by the movement of the cold air aloft associated with the CFA. From the resulting pressure gradient, the cross-isobaric acceleration and the cross-isobaric wind at the end of each time step can be calculated. Since the resulting winds were less than 10

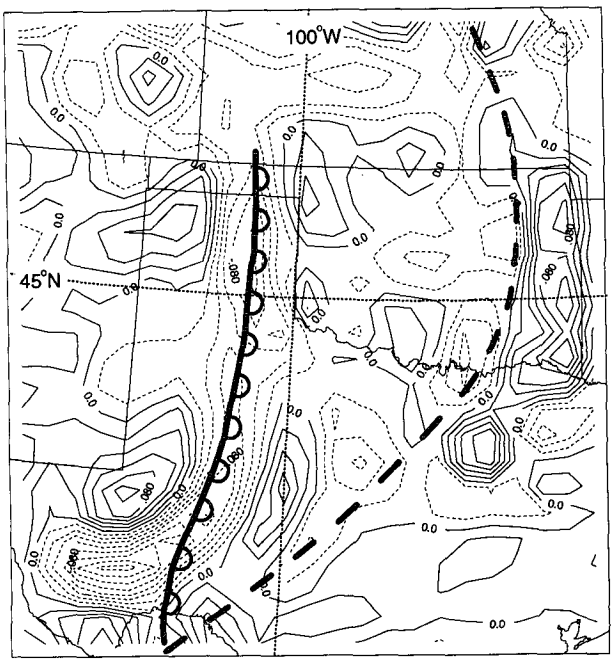

FIG. 16. As for Fig. 15 but for divergence (solid lines) and convergence (dashed lines) labeled in 10^{-2} s^{-1} and contoured every 2 × 10^{-4} s^{-1}.

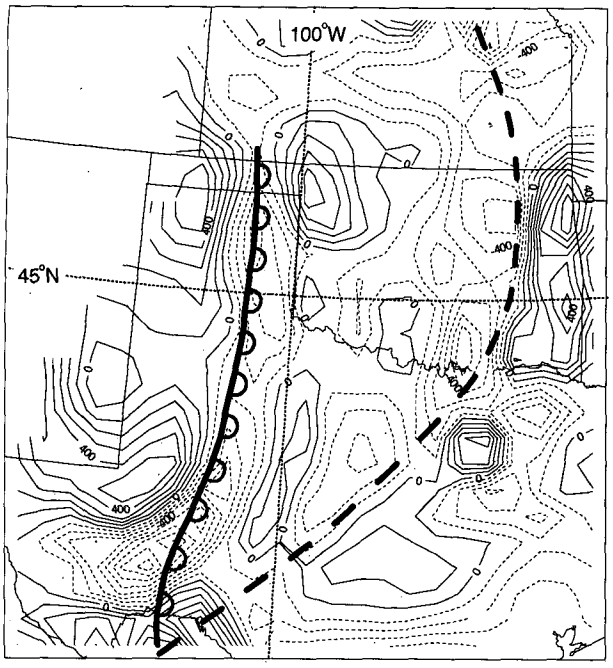

FIG. 17. Upward vertical air motions (dashed lines) and downward vertical air motions (solid lines), labeled in 10^{-5} hPa s^{-1} and contoured every 10^{-3} hPa s^{-1}, at 850 hPa at 0300 UTC 9 March 1992.

m s^{-1} and the time step was only 5000 s, we assumed that the Coriolis force would not significantly change the magnitude of the cross-isobaric wind. We also assumed that mass transfer from the convergence would not significantly affect the pressure field. Using the cross-isobaric wind, we derived the vertical air velocity by integrating the mass convergence form of the continuity equation.

Figure 18 shows a portion of the calculation domain at the end of the first time step. The resulting temperature distribution, the surface pressure pattern, and some values of cross-isobaric winds, convergence, and vertical velocity are shown in this figure. The regions of strongest upward vertical motion ($\sim$15–32 cm s^{-1}) occurred below and slightly behind the nose of the CFA. The vertical velocities at 1.5 km are larger but not appreciably different from those derived from the MM4 model at 850 hPa. We conclude that the intrusion of the CFA and the concurrent rate of change of the pressure gradient provided significant upward motion in the lower troposphere in a narrow band that was coincident with the nose of the CFA.

In section 3a we showed that prior to the passage of the CFA the lower levels of the atmosphere were potentially unstable and close to becoming absolutely unstable. If vertical motions on the order of 20 cm s^{-1} were applied to this potentially unstable air over the course of 5000 s by the mechanism described above, absolute instability would have been produced.

We conclude that quasigeostrophic frontogenesis lifted air primarily ahead of the elevated nose of the cold-air advection aloft. From the surface up to the base of the cold air aloft changes in the horizontal pressure gradient produced by the passage of the CFA were primarily responsible for the lifting of the air. We propose that the initial trigger for the CFA rainband was convergence below the leading edge of cold-air advection; since this convergence was concentrated below the nose of the CFA in the potentially unstable layer, it would have lifted the entire layer. This process was enhanced by lifting aloft at the nose of the CFA. Together these processes provided ample lifting throughout the troposphere to maintain the CFA rainband.

5. Discussion and summary

It is well established that the elevated cold baroclinic zones of warm occlusions are often associated with significant upward vertical air motions, clouds, and precipitation that produce a rainband along the leading edge of the cold baroclinic zone and changes in the rate of fall of pressure at the surface as the rainband passes overhead (e.g., Kreitzberg and Brown 1970; Houze et al. 1976; Hobbs and Locatelli 1978; Matejka et al. 1980; Matkovskii and Shakina 1982). It is not surprising, therefore, that cold baroclinic zones aloft or cold frontogenesis aloft (CFA) in warm occluded-like structures east of the Rocky Mountains are also associated with rainbands. In this paper we have described one such rainband, which took the form of a series of squall lines that produced severe weather. Other examples have been described by Locatelli et al. (1989), Sienkiewicz et al. (1989), Geerts and Hobbs (1991), Martin et al. (1990), Hobbs et al. (1990), and Steenburgh and Mass (1994).

However, there are important differences between the occluded-like structures that occur east of the Rockies and their oceanic counterparts. As a region of CFA approaches the position of a lee trough over the western slopes of the Great Plains, the warm frontal–like circulation associated with the lee trough superimposes subsiding air off the Rocky Mountains over air moving north that is located east of the lee trough. If the lee trough has the characteristics of a dryline (so that it forms a drytrough), then the warm frontal–like circulation superimposes warm dry (low θ_e) air from the high plateaus and subsiding air off the Rocky Mountains over warm moist (high θ_e) air from the Gulf of Mexico in an upward-sloping zone that is characterized by extreme potential instability (Fig. 19a). As the CFA interacts with the drytrough, it tips forward to form an occluded-like structure (in which the drytrough is analogous to the warm-frontal portion of a classical occlusion). Two regions of upward motion are associated with the CFA (Fig. 19b). The higher region, which is situated ahead and above the nose of the CFA, is the upward branch of the thermally direct circulation that

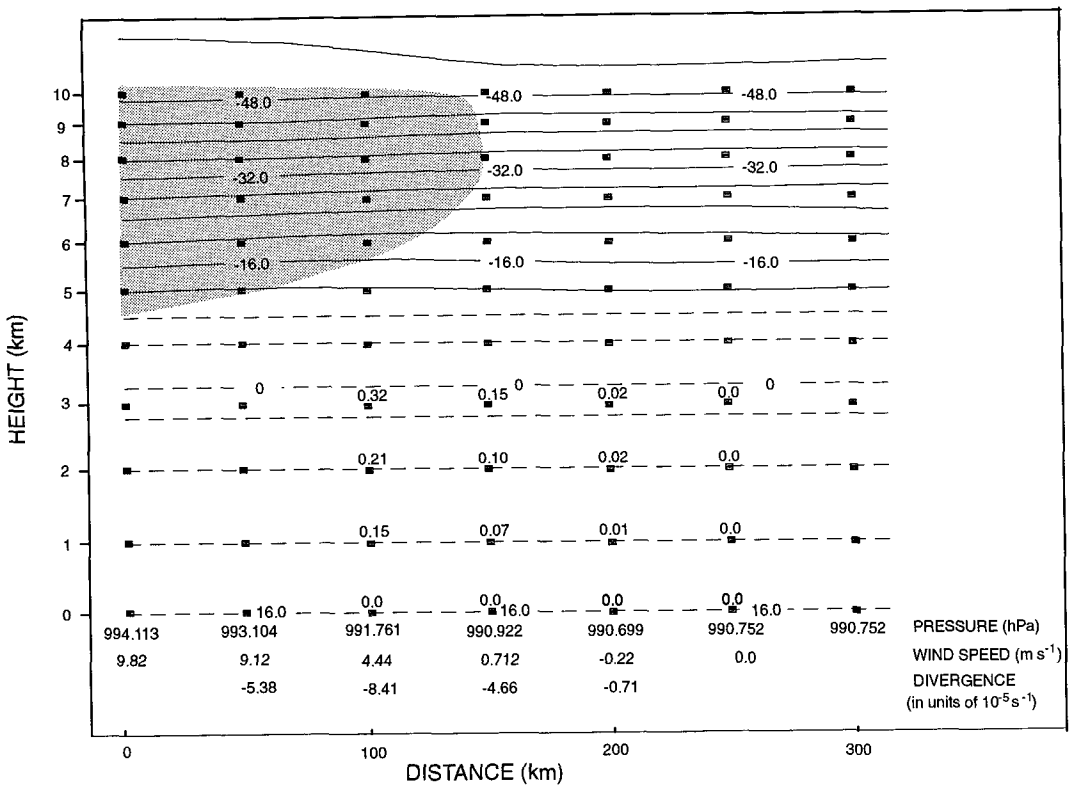

FIG. 18. Cross section showing 2D numerical model results at the end of the first time step. The solid lines are isotherms from MM4 model simulations at 0300 UTC 9 March 1992. The dashed lines are isotherms. Model calculated vertical velocities (m s^{-1}) are shown above the grid points. Pressure (hPa), wind speed (m s^{-1}), and divergence (10^{-5} s^{-1}) at the surface are listed below each surface grid point. The region of the cold-air advection aloft is shown by the shading.

is maintained by frontogenesis. The lower region of upward motion is the result of rapid changes in the pressure gradient beneath the nose of the CFA as it passes overhead. This produces ageostrophic winds and convergence as air parcels adjust to the changing pressure gradient. As the potentially unstable air mass is lifted to saturation, it triggers the formation of a convective CFA rainband, which moves eastward with the CFA, away from the drytrough (Fig. 19c). By contrast, the rainbands associated with cold baroclinic zones aloft in classic warm occlusions are generally stratiform in nature.

Browning (1985) suggested that the upper cold fronts of split fronts are a major cause of squall lines in the central United States. Browning was correct in the sense that CFA (or upper cold fronts in Browning's terminology) can cause squall lines. However, the CFA structures described in this paper are not split fronts (i.e., a cold front aloft over a warm sector), nor did they form in the manner described by Browning and Monk (1982). Instead, the structures we have described are like warm occlusions in which a lee trough (or drytrough in some cases) east of the Rocky Mountains acts as the surface warm front (Locatelli et al. 1989; Hobbs et al. 1990; Steenburgh and Mass 1994). Thus, in these systems the region analogous to the classic warm sector of a warm occlusion is located west of the surface position of the lee trough, not east of it as required by the split-front model. Figure 20 summarizes the essential differences between the split-front model and our model for CFA. In Fig. 20a (split front) the broad darker-shaded arrow represents the conveyor belt (high-θ_w flow), which, relative to the moving system, travels ahead of the surface cold front within the warm sector before rising and turning to the right above a warm-frontal zone. The lighter-shaded arrows represent dry air (low-θ_w flow); this air overruns the conveyor belt, and its leading edge marks the position of the upper cold front. In Fig. 20b (CFA model) the broad darkest-shaded arrow represents the conveyor belt (high-θ_w flow), which, relative to the moving system, travels ahead of the surface lee trough before rising and turning to the right in a warm frontal–like zone. The medium-shaded arrow represents low-θ_w air that, relative to the moving system, moves over the lee trough, rising and turning to the right above the high-θ_w flow. The lightest-shaded arrows represent dry cool air (low-θ_w flow); this air overruns the other two

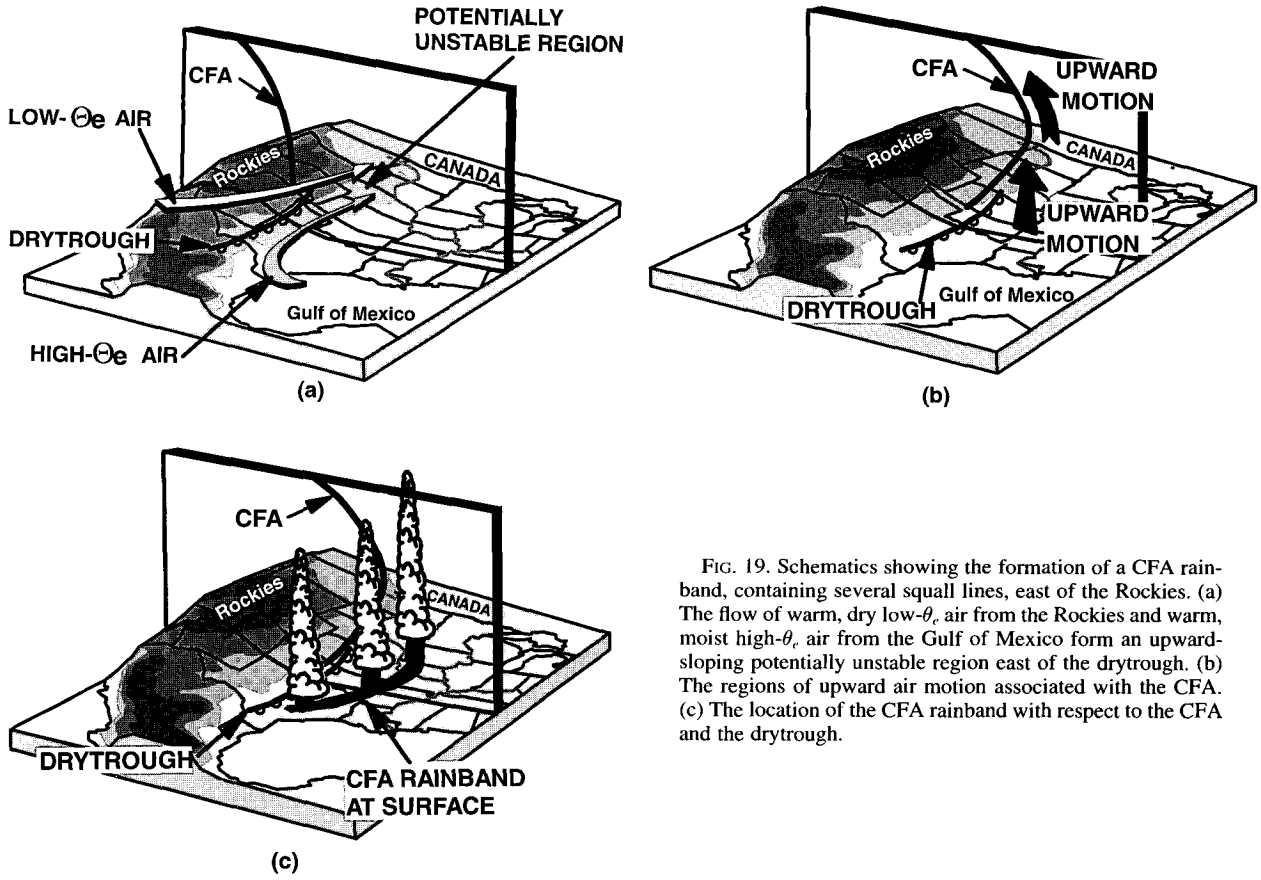

FIG. 19. Schematics showing the formation of a CFA rainband, containing several squall lines, east of the Rockies. (a) The flow of warm, dry low-θ_e air from the Rockies and warm, moist high-θ_e air from the Gulf of Mexico form an upward-sloping potentially unstable region east of the drytrough. (b) The regions of upward air motion associated with the CFA. (c) The location of the CFA rainband with respect to the CFA and the drytrough.

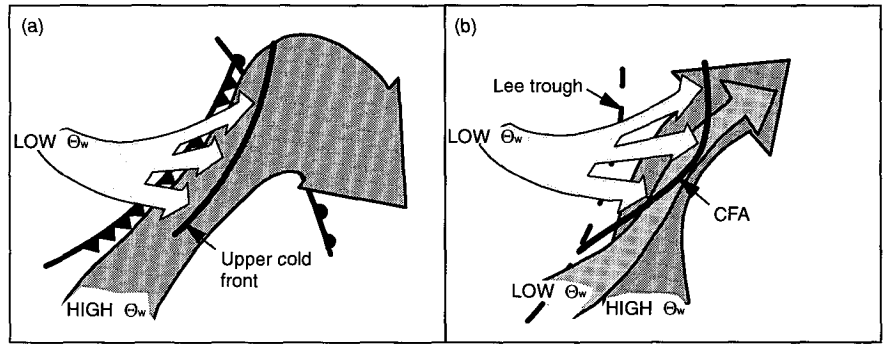

FIG. 20. (a) Schematic portrayal of a split front in plan view adapted from Browning and Monk (1982). The broad darker shaded arrow represents the conveyor belt (high-θ_w flow), which, relative to the moving system, travels ahead of the surface cold front before rising and turning to the right above a warm-frontal zone. The lighter-shaded arrows represent dry air (low-θ_w flow); this air overruns the conveyor belt, and its leading edge marks the position of the upper cold front. Surface fronts are shown by standard symbols. (b) Schematic plan view of the CFA model. The broad darkest-shaded arrow represents the conveyor belt (high-θ_w flow), which, relative to the moving system, travels ahead of the surface lee trough before rising and turning to the right in a warm frontal–like zone. The medium-shaded arrow represents low-θ_w air that, relative to the moving system, moves over the lee trough, rising and turning to the right above the high-θ_w flow. The lightest-shaded arrows represent dry cool air (low-θ_w flow); this air overruns the other two airflows, and its leading edge marks the position of the CFA.

airflows, and its leading edge marks the position of the CFA.

Early research, such as that of Crawford (1950), Armstrong (1953), and Omoto (1965), showed that cold baroclinic zones aloft (i.e., CFA) were an important factor in the formation of severe weather east of the Rocky Mountains. More recent research (referenced previously in this paper), which has focused on detailed case studies in which CFA rainbands were associated with severe weather and squall lines, supports this view.

In this paper we have shown that the dynamics of CFA can lift potentially unstable stratified air masses and trigger severe convection and squall lines. Subsequently, the structure of the CFA is ideally suited to sustain a squall line. The synoptic-scale pool of cool dry air behind the nose of the CFA is a source of low-θ_e air, which supplies the rear inflow air that is needed to evaporate precipitation and maintain the squall line (e.g., Smull and Houze 1985). Also, the cooling produced by the evaporation of precipitation in the dry air behind the CFA and the release of latent heat ahead of the CFA can strengthen the CFA. We surmise that the whole system acts in a synergistic way to lock the squall line to the CFA: as the CFA triggers the squall line, the dynamics and thermodynamics of the squall line strengthen the CFA, which further strengthens the squall line.

We conclude that CFA provides a major triggering and sustaining mechanism for severe weather (squall lines and tornadoes) in the central United States in winter and early spring. Since operational weather forecasting numerical models (e.g., the NWS Nested Grid Model) and mesoscale research models (e.g., the Penn State–NCAR MM4 and MM5 models) can predict the location and movement of CFA [see, e.g., Hobbs et al. (1990); and section 2 of this paper], the interpretation of these model outputs in light of the importance of CFA should lead to improved forecasts of severe weather in the central United States.

Acknowledgments. We thank all the participants of STORM-FEST for help in collecting specialized datasets. We are grateful to Mark Stoelinga for help in reducing the Penn State–NCAR MM4 model pressure data. This research was supported by Grant ATM-9106235 from the Atmospheric Research Division of the National Science Foundation.

REFERENCES

Anthes, R. A., and T. T. Warner, 1978: Development of hydrodynamic models suitable for air pollution and other meso-meteorological studies. *Mon. Wea. Rev.*, **106,** 1045–1078.

——, E.-Y. Hsie, and Y.-H. Kuo, 1987: Description of the Penn State/NCAR Mesoscale Model Version (MM4). NCAR Tech. Note NCAR/TN-282+STR, 66 pp.

Armstrong, H., 1953: Forecasting of tornadoes in Georgia. *Mon. Wea. Rev.*, **81,** 290–298.

Blackadar, A. K., 1979: High resolution models of the planetary boundary layer. *Advances in Environmental Science and Engineering,* 1, No. 1, Pffafflin and Zeigler, Eds., Gordon and Breach Scientific Publishers, 50–85.

Browning, K. A., 1985: Conceptual models of precipitation systems. *Meteor. Mag.*, **114,** 293–319.

——, and G. A. Monk, 1982: A simple model for the synoptic analysis of cold fronts. *Quart. J. Roy. Meteor. Soc.*, **108,** 435–452.

Crawford, M. E., 1950: A synoptic study of squall lines. *Bull. Amer. Meteor. Soc.*, **31,** 351–357.

Fujita, T., 1992: *Mystery of Severe Storms.* Wind Research Laboratory, Department of Geophysical Sciences, University of Chicago, 298 pp.

Geerts, B., and P. V. Hobbs, 1991: The organization and structure of cloud and precipitation on the mid-Atlantic coast of the United States. Part IV: Retrieval of the thermodynamics and cloud microphysical structures of a frontal rainband from Doppler radar data. *J. Atmos. Sci.*, **48,** 1287–1305.

Hobbs, P. V., and J. D. Locatelli, 1978: Rainbands, precipitation cores and generating cells in a cyclonic storm. *J. Atmos. Sci.*, **35,** 230–241.

——, ——, and J. E. Martin, 1990: Cold fronts aloft and the forecasting of precipitation and severe weather east of the Rocky Mountains. *Wea. Forecasting,* **5,** 613–626.

Holzman, B., 1936: Synoptic determination and forecasting significance of cold fronts. *Mon. Wea. Rev.*, **64,** 400–413.

Hoskins, B. J., I. Draghici, and H. C. Davies, 1978: A new look at the ω-equation. *Quart. J. Roy. Meteor. Soc.*, **104,** 31–38.

Houze, R. A., Jr., J. D. Locatelli, and P. V. Hobbs, 1976: Dynamics and cloud microphysics of the rainbands in an occluded frontal system. *J. Atmos. Sci.*, **33,** 1921–1936.

Keyser, D., and T. N. Carlson, 1984: Transverse ageostrophic circulations associated with elevated mixed layers. *Mon. Wea. Rev.*, **112,** 2465–2478.

——, and M. A. Shapiro, 1986: A review of the structure and dynamics of upper level frontal zones. *Mon. Wea. Rev.*, **114,** 452–499.

Kreitzberg, C. W., and H. A. Brown, 1970: Mesoscale weather systems within an occlusion. *J. Appl. Meteor.*, **9,** 417–432.

Lichtblau, S., 1936: Upper cold fronts in North America. *Mon. Wea. Rev.*, **64,** 414–425.

Lloyd, J. R., 1942: The development and trajectories of tornadoes. *Mon. Wea. Rev.*, **70,** 65–75.

Locatelli, J. D., J. M. Sienkiewicz, and P. V. Hobbs, 1989: Organization and structure of clouds and precipitation on the mid-Atlantic coast of the United States. Part I: Synoptic evolution of a frontal system from the Rockies to the Atlantic Coast. *J. Atmos. Sci.*, **46,** 1327–1348.

Martin, J. E., J. D. Locatelli, and P. V. Hobbs, 1990: Organization and structure of clouds and precipitation on the mid-Atlantic coast of the United States. Part III: The evolution of a middle-tropospheric cold front. *Mon. Wea. Rev.*, **118,** 195–217.

——, ——, and ——, 1992: Organization and structure of clouds and precipitation on the mid-Atlantic coast of the United States. Part V: The role of an upper-level front in the generation of a rainband. *J. Atmos. Sci.*, **49,** 1293–1303.

——, ——, ——, P.-Y. Wang, and J. Castle, 1995: Structure and evolution of winter cyclones in the central United States and their effects on the distribution of precipitation. Part I: A synoptic-scale rainband associated with a dryline and lee trough. *Mon. Wea. Rev.*, **123,** 241–264.

Matejka, T. J., R. A. House Jr., and P. V. Hobbs, 1980: Microphysics and dynamic of clouds associated with mesoscale rainbands in extratropical cyclones. *Quart. J. Roy. Meteor. Soc.*, **106,** 29–56.

Matkovskii, B. M., and N. P. Shakina, 1982: Mesoscale structure of an occluded front over the center of the European USSR from special measurements. *Meteor. Gidrol.*, **1,** 24–33.

Moore, J. T., and P. D. Blakely, 1988: The role of frontogenetic forcing and conditional symmetric instability in the Midwest snowstorm of 30–31 January 1982. *Mon. Wea. Rev.*, **116,** 2155–2171.

Newton, C. W., 1950: Structure and mechanisms of the prefrontal squall line. *J. Meteor.*, **7,** 210–222.

Omoto, Y., 1965: On pre-frontal precipitation zones in the United States. *J. Meteor. Soc. Japan,* **43,** 310–330.

Sanders, F., and L. F. Bosart, 1985: Mesoscale structure in the megalopolitan snowstorm of 11–12 February 1983. Part I: Frontogenetical forcing and symmetric instability. *J. Atmos. Sci.,* **42,** 1050–1061.

——, and B. J. Hoskins, 1990: An easy method for estimation of *Q*-vectors from weather maps. *Wea. Forecasting,* **5,** 346–353.

Sienkiewicz, J. M., J. D. Locatelli, P. V. Hobbs, and B. Geerts, 1989: Organization and structure of clouds and precipitation on the mid-Atlantic coast of the United States. Part II: The mesoscale and microscale structure of some frontal rainbands. *J. Atmos. Sci.,* **46,** 1349–1364.

Smull, B. F., and R. A. Houze Jr., 1985: A midlatitude squall line with a trailing region of stratiform precipitation: Radar and satellite observations. *Mon. Wea. Rev.,* **113,** 117–133.

Steenburgh, W. J., and C. F. Mass, 1994: The structure and evolution of a simulated Rocky Mountain lee trough. *Mon. Wea. Rev.,* **122,** 2740–2761.

Wallace, J. M., and P. V. Hobbs, 1977: *Atmospheric Science: An Introductory Survey.* Academic Press, 467 pp.

Williams, D. T., 1953: Pressure wave observations in the central Midwest, 1952. *Mon. Wea. Rev.,* **81,** 278–289.

Zhang, D.-L., and R. A. Anthes, 1982: A high-resolution model of the planetary boundary layer: Sensitivity tests and comparisons with SESAME-79 data. *J. Appl. Meteor.,* **21,** 1594–1609.